nature astronomy

REVIEW ARTICLE

https://doi.org/10.1038/s41550-021-01580-0

Gamma-ray haloes around pulsars as the key to understanding cosmic-ray transport in the Galaxy

Rubén López-Coto[1,2] ✉, Emma de Oña Wilhelmi[3] ✉, Felix Aharonian[4,5], Elena Amato[6,7] and Jim Hinton[4]

Pulsars are factories of relativistic electrons and positrons that propagate away from the pulsar, eventually permeating our Galaxy. The acceleration and propagation of these cosmic particles are a matter of intense debate. In the last few years, we have had the opportunity to directly observe the injection of these particles into the interstellar medium through the discovery of gamma-ray haloes around pulsars. This new type of gamma-ray source is produced by electrons and positrons diffusing out of the pulsar wind nebula and scattering ambient photon fields to produce gamma rays. This correspondingly new field of study comes with a number of observations and constraints at different wavelengths and a variety of theoretical models that can explain the properties of these haloes. We examine the characteristics of the propagation of cosmic rays inferred from the observations of gamma-ray haloes and their local and global implications for particle transport within the Galaxy. We also discuss the prospects for observations of these sources with facilities such as the Large High Altitude Air Shower Observatory, the Cherenkov Telescope Array or the Southern Wide-field Gamma-ray Observatory in the near future.

Pulsars, rapidly rotating neutron stars left behind in supernova explosions, have played a critical role in the development of many areas of astrophysics. In non-thermal astrophysics, the nebula around the Crab pulsar was the first known teraelectronvolt source[1] and is by far the best-studied site of astrophysical particle acceleration outside the Solar System[2,3]. The relativistic wind from pulsars is halted at a termination shock (TS), and beyond this a synchrotron-radiation-emitting pulsar wind nebula (PWN) forms, apparently dominated by relativistic electron–positron pairs and magnetic fields (see ref. [4] for a review). The processes of energy conversion from the highly magnetized flow in the vicinity of the pulsar magnetosphere (at ~10^6 m) to the particle-dominated one at the parsec-scale nebula are a matter of continuing debate and intense theoretical study (see, e.g., ref. [5] and references therein).

Ideally, in a steady, spherical flow, the gamma radiation from the confined region should reflect the dominant convective character of propagation (relativistic magnetohydrodynamic—MHD—flow) and the morphology of the nebula (typically elongated/asymmetric relative to the pulsar's position), whereas beyond it a diffusive propagation should dominate. Note however that this paradigm breaks when looking at the emission of the highest-energy particles, which, especially in evolved objects, have large Larmor radii that can be comparable to the system size (more complex MHD simulations and particle transport models are required when looking into PWNes in detail[6–8].

Figure 1 illustrates the main evolutionary stages of PWNe. During stage 1 the PWN is inside the supernova remnant (SNR) and has not yet been touched by the reverse shock. Stage 2 starts when the PWN is crushed by the reverse shock but the pulsar is still within the SNR: due to the declining magnetic field and the different cooling time of the emitting electrons, X-ray-dim, gamma-ray-bright 'relic' bubbles can be observed at this stage. Stage 3 starts when the pulsar leaves its parent SNR and high-energy particles escape into the interstellar medium (ISM): Geminga and PSR B0656+14[9] are thought to be in this stage. The fringes between stages 2 and 3 are often unclear, and there has been considerable discussion of when the term 'halo' can legitimately be applied. Here we adopt the term to refer to a population of particles essentially free from their parent PWN, or at least outside the region in which the nebula is energetically dominant.

Understanding the physics of these haloes has implications of fundamental importance for a number of open problems in high-energy astrophysics. First, haloes can be used to probe the evolution of particle acceleration and escape in pulsars and PWNe, which are themselves a unique laboratory for relativistic astrophysics. Second, the observation of cooling electrons and positrons travelling freely through the ISM from a well defined source provides a unique probe of the propagation of relativistic particles. This transport is regulated by the diffusion coefficient, which for the ISM has been estimated to be $D(10\,\mathrm{GeV}) \sim 8\times10^{28}\,\mathrm{cm^2\,s^{-1}}$ (refs. [10,11]), through comparison between spallation data and particle transport models. However, this value refers to the average diffusion coefficient in the ISM, and local variations should be expected. Observations of haloes provide information about these variations around powerful electron and positron accelerators. Moreover, these measurements have strong implications for the global electron spectrum.

In this Review, we explore the existing experimental constraints on pulsar haloes and discuss the theoretical expectations for particle escape and propagation, finally considering the prospects in this area given the powerful new instrumentation on the horizon.

Current experimental results

The observations of our Galaxy in the teraelectronvolt energy range with moderate- to large-field-of-view sensitive telescopes have revealed a large number of extended regions of gamma rays. In particular, the Galactic plane survey performed by the High Energy Stereoscopic System (H.E.S.S.) array of Cherenkov telescopes[12–14] was a milestone in the study of such multiparsec structures, unveiling a large population of PWNe, which dominates the

[1]Istituto Nazionale di Fisica Nucleare, Sezione di Padova, Padova, Italy. [2]Instituto de Astrofísica de Andalucía, CSIC, Granada, Spain. [3]DESY, Zeuthen, Germany. [4]Max-Planck-Institut für Kernphysik, Heidelberg, Germany. [5]Dublin Institute for Advanced Studies, Dublin, Ireland. [6]INAF, Osservatorio Astrofisico di Arcetri, Firenze, Italy. [7]Università degli Studi di Firenze, Sesto Fiorentino (FI), Italy. ✉e-mail: rlopezcoto@gmail.com; emma.de.ona.wilhelmi@desy.de

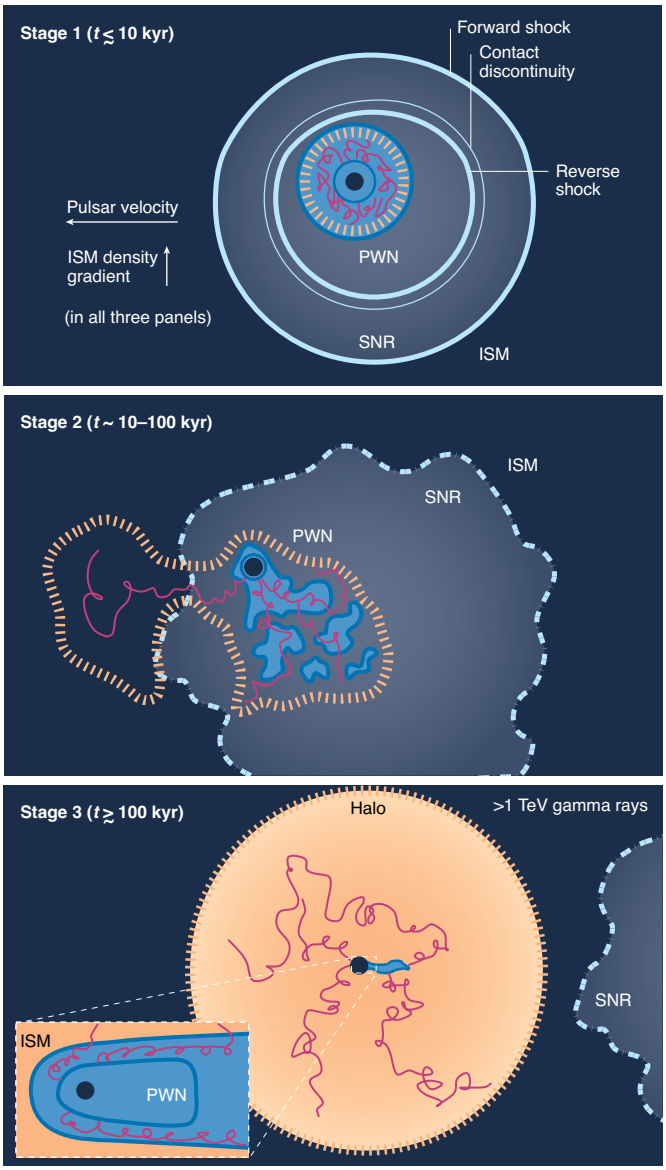

Fig. 1 | Evolutionary stages in the life of a PWN. The early confinement of particles and the later escape of (at least) the higher-energy relativistic particles to form a halo visible in teraelectronvolt gamma rays is illustrated. Figure adapted from ref. [28] under Creative Commons license CC BY 4.0.

teraelectronvolt emission of the Galactic plane[15]. The presence of teraelectronvolt structures much larger than the X-ray ones had already been predicted in ref. [16]. The large diversity of teraelectronvolt PWNe discovered by H.E.S.S. and other Imaging Atmospheric Cherenkov Telescopes such as VERITAS (Very Energetic Radiation Imaging Telescope Array System) and MAGIC (Major Atmospheric Gamma Imaging Cherenkov Telescopes) (see, e.g., refs. [17,18]) promoted the classification of PWN evolution in several stages, according to the physical properties of the region from which teraelectronvolt emission originates during the lifetime of a pulsar. This first classification included a free-expansion stage, followed by a second phase in which the PWN is interacting with the turbulent plasma left behind by the SN explosion (stage 1 in Fig. 1); examples of this stage are PWNe such as the Crab Nebula or 3C 58. The next stage, also called the relic stage, is one in which a large teraelectronvolt nebula expands beyond the SNR, altering the surrounding ISM (stage 2 in Fig. 1). For objects in this stage, teraelectronvolt observations with Cherenkov telescopes, combining good energy and angular resolution, allowed disentanglement between emission properties in different subregions, proving efficient particle cooling and diffusive propagation within the nebula[19–22].

The advent of large-field-of view instruments such as Milagro[23] and currently the High-Altitude Water Cherenkov Observatory (HAWC) and Large High Altitude Air Shower Observatory (LHAASO) in the teraelectronvolt range[24,25], and the Fermi-LAT (Large Area Telescope) satellite in the gigaelectronvolt range[26], opened a new window to complete the evolutionary picture of PWNe, thanks to improved sensitivity to very large gamma-ray structures (Fig. 2). The discovery of a large ~5° teraelectronvolt emission around the ≳100-kyr-old pulsars Geminga and PSR B0656+14 triggered a new understanding of the electrons injected within the pulsar environment. The dimension of the halo (~25 pc for 100 TeV electrons) has been interpreted as due to slow escape[9] of electrons and positrons accelerated at the pulsar wind TS. The most natural explanation for the propagation is that charged particles diffuse in the turbulent magnetic field of the region. Under this assumption, ref. [9] constrained the diffusion coefficient in the region surrounding Geminga and PSR B0656+14 to $D(100\,\mathrm{TeV}) \sim 5 \times 10^{27}\,\mathrm{cm^2\,s^{-1}}$, a value much lower than the average in the ISM, which poses a problem for the origin of this increased level of turbulence with respect to that inferred, from local cosmic-ray spectra, as the average in the Galaxy. Recently, an alternative interpretation to the slow-diffusion scenario has been proposed, in which a combination of ballistic plus diffusive propagation at the same rate as the average in the ISM is used to explain the observed size and teraelectronvolt emission features[27]. The region seen in the teraelectronvolt range is characterized by an energy density below that of the ISM, which exhibits an outflow of escaping electrons in a region that is not modified by the pulsar itself. The proximity of these pulsars (at ~250 pc), combined with the large field of view, makes possible the detection of the otherwise very low teraelectronvolt gamma-ray surface brightness ($\sim 10^{-12}\,\mathrm{TeV\,cm^{-2}\,s\,deg^{-2}}$). These electrons diffuse away and fill up a large region or halo, providing a unique clean scenario to study diffusive propagation in the Galaxy. The transition between relic and halo stages is blurred and has motivated different classification criteria[28,29]. An example of this transitional stage is the very extended source HESS J1825-137 (21 kyr), with an unusually large extension of ≳100 pc (refs. [30,31]), exceeding the scales anticipated by the standard hydrodynamical paradigm of PWN formation. The energy dependence of the morphology strongly suggests advection-dominated transport within the PWN, but the fringes of the emission extend to very large distances and may indicate the presence of unconfined teraelectronvolt-emitting particles[30]. Similarly, the 11-kyr-old Vela X shows a compact teraelectronvolt emission, coincident with a bright X-ray nebula and an extended region with a similar spectrum. The extended region also coincides with a radio halo[32], which might be a sign of particles escaping[20,33–35]. However, the majority of the teraelectronvolt PWNe are consistent with a relic scenario. These naturally stem from the observational bias towards ~0.2° sources at ~5 kpc distance, for which Cherenkov telescope sensitivity is optimal, in terms of size and flux: at shorter distances the halo becomes too large to be fully contained in the field of view[36–38], whereas for distant sources the flux might be too faint to be detectable. The good angular resolution permits however a deeper investigation of the morphology in different energy ranges, hinting at transition regions between different propagation regimes. Although there are only two firmly identified sources in which emission is produced by already escaped electrons, there have been reports of other halo candidates[39–43] and proposals that this could be the dominant mechanism in several known sources[44,45]. Very recently, the LHAASO collaboration has reported the detection of Geminga[46] and is currently studying it and PSR B0656+14 in detail[47].

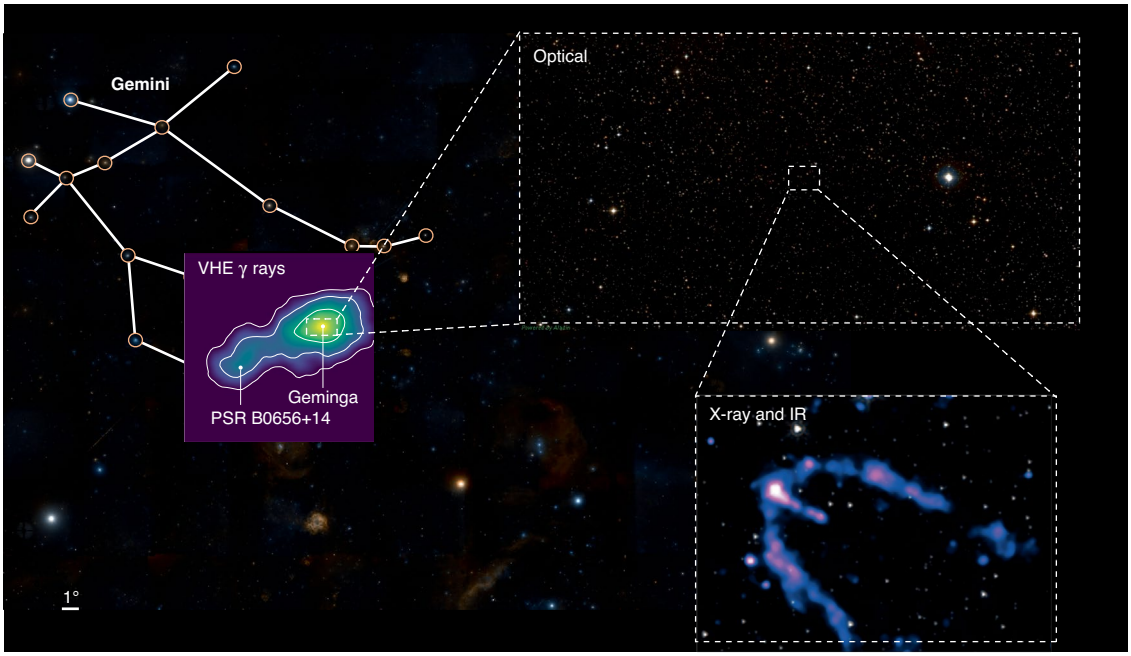

Fig. 2 | Map of the sky region around the HAWC detection of Geminga. Background image and 'Optical' inset: DSS2 obtained using Aladin sky atlas (ref. [9]; original source, Palomar Observatory/California Institute of Technology). Very high energy gamma-ray inset: test-statistics map adapted with permission from the HAWC observations (ref. [9], AAAS). 'X-ray and IR' inset: X-ray, NASA/CXC/PSU/ref. [49]; IR map, NASA/JPL-Caltech.

The observation of the multiwavelength counterpart of pulsar haloes poses severe challenges. The corresponding size and expected flux are related to the particles' cooling regime: in the sub-100-GeV and radio energy band a large emission region with a very hard spectral index is expected, whereas the highest-energy electrons are affected by strong cooling, resulting in compact soft X-ray emission (Fig. 2), as in the case of Geminga[48,49]. Geminga has been investigated in the gigaelectronvolt regime by several authors using data from the Fermi-LAT. The results are however hampered by the expected number of photons in this energy band: on one hand, the hard uncooled electron spectrum (~1.8) results in low flux levels below a few tens of gigaelectronvolts; on the other hand, the overwhelming gamma-ray background diffuse emission that dominates the Galactic plane makes it difficult to disentangle the low surface brightness of these haloes. Using an energy-dependent, model-dependent template, ref. [50] claimed a detection of the Geminga halo above 10 GeV . A second analysis in ref. [51], using a smaller region of interest, did not confirm such an extended gigaelectronvolt emission, using a similar physics-motivated template approach (two-zone diffusion spatial templates), although not including the proper motion of the pulsar. Observations with instruments such as the Cherenkov Telescope Array (CTA) or Southern Wide-field Gamma-ray Observatory (SWGO) in the future should provide a clear picture of the evolution in size and spectrum below hundreds of gigaelectronvolts.

In the search for haloes, X-ray observations provide different diagnostic tools at different scales. On one hand, the excellent angular resolution of instruments such as X-ray Multi-Mirror Mission (XMM)-Newton and Chandra provides precise images of pulsars propagating in the ISM, forming a bow-shock, which demonstrates particle escape through the observation of bright filaments[52–54]. On the other, a few-degree soft-X-ray halo should emerge, corresponding to the synchrotron emission of electrons powering the gamma-ray source. The detection of such diffuse emission requires a deep-observation programme involving several pointings. In the case of Geminga, ref. [55] examined a 1° region around the pulsar and obtained an upper limit on the magnetic field below 1 μG, based on X-ray upper limits on the synchrotron emission by the electrons responsible for the emission detected by HAWC. The derived magnetic field is below the mean one in the ISM, pointing to a perturbed medium.

Implications in PWN theory

The experimental results described above have several implications, regarding not only the acceleration efficiency of particles (electrons and positrons) but also their propagation. The maximum particle energy derived from the highest photon energy measured in Geminga (≈300 TeV) has strong implications in the acceleration mechanisms: it appears that particles are accelerated up to a fraction close to 1 of the maximum potential drop available in the pulsar magnetosphere $\Phi_{\rm PSR} = \sqrt{\dot{E}/c}$ (ref. [56]), with c the speed of light and $\dot{E}$ the pulsar spin-down power. The bulk of the particles making PWNe bright non-thermal sources are believed to be accelerated at the pulsar wind TS. The details of the mechanisms are not clear. The three main proposals are shock acceleration (see ref. [57] for a review), magnetic reconnection[58] and resonant absorption of ion cyclotron waves[59,60]. All of these mechanisms may in principle reach the required energies (see, e.g., ref. [61] for a recent review), but not easily. In fact, the maximum achievable energy at the TS (ignoring all dissipative effects) is determined by the condition that the particle Larmor radius be smaller than the characteristic size of the accelerator ('Hillas criterion'), namely $E_{\rm max,TS} = eR_{\rm TS}B_{\rm TS}$, where $R_{\rm TS}$ is the TS radius and $B_{\rm TS}$ the local magnetic field strength. Writing the magnetic pressure at the TS as a fraction η_B of the ram pressure of the wind $\dot{E}/(4\pi R_{\rm TS}^2 c)$, we find $B_{\rm TS} = (\eta_B^{1/2}/R_{\rm TS})\sqrt{\dot{E}/c}$, from which we derive that the maximum achievable energy at the TS ($\eta_B = 1$) is $E_{\rm max,TS} \approx e\Phi_{\rm PSR}$; that is, in the absence of losses, the maximum energy depends only on the potential drop in the pulsar magnetosphere. Note that this constraint does not depend on the acceleration mechanism. Writing the pulsar spin-down luminosity in units of $10^{36}\,{\rm erg\,s^{-1}}$, we have $E_{\rm max} \approx 1.8\eta_B^{1/2}\dot{E}_{36}^{1/2}$ PeV (with $\dot{E}_{36}$ in units of $10^{36}\,{\rm erg\,s^{-1}}$). In particular, for Geminga, with $\dot{E}_{36} = 0.03$, electron

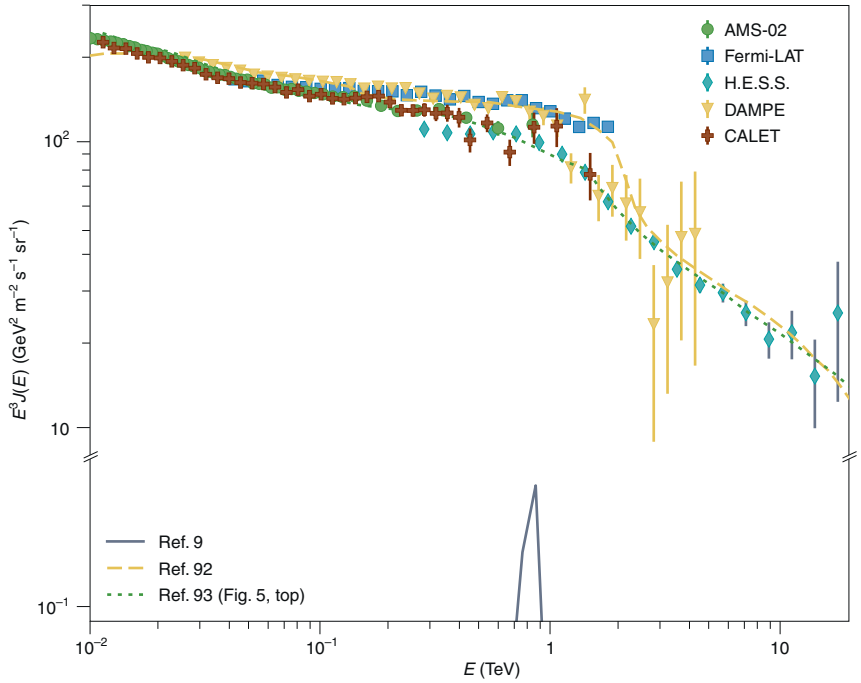

Fig. 3 | Local all-electron spectrum. Data from AMS-02[94], the Calorimetric Electron Telescope (CALET)[91], the Dark Matter Particle Explorer (DAMPE)[90], Fermi-LAT[107] and H.E.S.S.[89], together with predictions from refs. [92,93], and the flux inferred in ref. [9]. Error bars represent 1σ statistical errors in the data points.

energies of a few hundred teraelectronvolts correspond to maximally efficient acceleration.

Once these particles have been accelerated, their escape in the ISM is again a dive into poorly understood physics. The common view of PWNe is that these sources can be well modelled within the framework of relativistic MHD (see, e.g., ref. [62] for a review), where the propagation of particles inside them is governed by advection. This picture is bound to fail at the highest energies, and indeed computation of the particle dynamics on top of the electromagnetic field structure derived from MHD simulations shows that only in a narrow energy range close to $E_{\rm max,TS}$ does the fraction of particles that can escape from a PWN become sizable[63]. Very interestingly, the escaping population is charge separated, with electrons and positrons escaping in approximately equal numbers, but along different paths[64]. In principle, this would create the conditions for the development, in the PWN vicinity, of a current large enough to have interesting consequences. In fact, one of the proposed explanations for the reduced diffusion coefficient constrained by the HAWC observations is that this results from an enhanced turbulence level produced by the particles escaping the PWN. The well-known resonant streaming instability[65] does not seem to be effective enough[66]. The existence of a net current opens the door to the possibility that the fast-growing non-resonant streaming instability[67] may be at work. This requires that the energy density in the current-carrying particles is larger than that in the local magnetic field. Such a condition, which it is possible in principle to satisfy[64], appears at odds with estimates of the energy density in very high-energy electrons derived from modelling of the Geminga halo emission[28]. An alternative explanation for the reduced diffusion coefficient is that it results from a local reduction of the magnetic field coherence length, down to parsec values, a factor $\approx 10^{-2}$ of what is commonly adopted for MHD turbulence in the Galaxy[68]. In fact, within quasilinear theory, the diffusion coefficient can be written as

$$D(E) \approx 2 \times 10^{28}\ \mathrm{cm^2\ s^{-1}}\ \xi_{B,0.1}^{-1} \left(\frac{\lambda_{\rm pc}}{E_{\rm TeV}}\right)^{\alpha-1} B_\mu^{\alpha-2} \qquad (1)$$

where $\xi_{B,0.1} = (\delta B/B)^2$ is the ratio between the power of the turbulent and ordered magnetic field normalized to 0.1, $\lambda_{\rm pc}$ is the outer scale of the turbulence in units of parsec, B_μ is the large-scale magnetic field in units of microgauss and $E_{\rm TeV}$ is the particle energy in teraelectronvolts; finally, α is the turbulence spectral index with $\alpha = 5/3$ (3/2) for a Kolmogorov (Kraichnan) phenomenology. It is clear then that a reduced diffusivity might result from an increased turbulence level (larger ξ_B) or a smaller coherence length λ of the turbulence. Distinguishing between these two scenarios would only be feasible by looking at particles of higher energies, with Larmor radii comparable to the turbulence coherence length. In that sense, observations with LHAASO should provide crucial information in the understanding of the diffusive regime. Recently, a new solution different from the diffusion-only regime for the propagation of electrons has been proposed. Reference [27] studied the halo morphology taking into account that a substantial fraction of the propagation of multi-teraelectronvolt electrons could take place in the ballistic or ballistic-to-diffusive regimes. The ballistic propagation of these electrons in a turbulent magnetic field for distances larger than their Larmor radius could make the gamma-ray morphology of Geminga compatible with the standard diffusion coefficient derived from cosmic-ray measurements.

Haloes and Galactic cosmic rays

The escaping particles diffuse further within the Galaxy, ultimately adding up to the sea of Galactic cosmic rays. These cosmic rays can be described as a low-density plasma whose propagation is governed by the diffusion-loss equation[69,70]. Local measurements of cosmic-ray fluxes and relative abundances provide insights into the distribution of sources generating them. What pulsar haloes directly probe is the transport of electrons and positrons, but since cosmic-ray propagation in the Galaxy is thought to depend on particle rigidity alone we expect the propagation of hadrons and leptons to be the same for a given rigidity. Irrespective of the cause of enhanced scattering in the haloes, these regions can have important implications for the galactic transport of both leptonic and hadronic

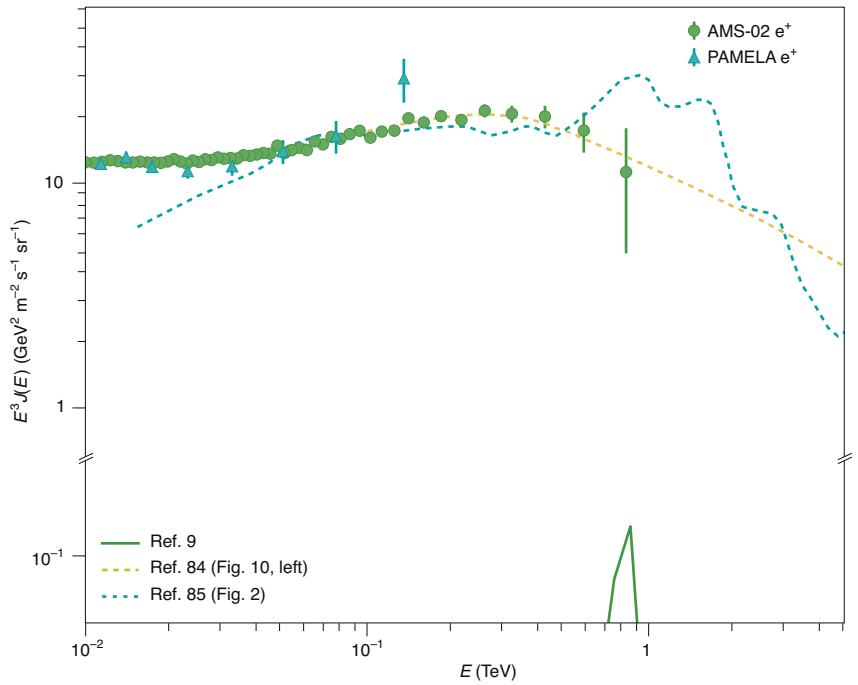

Fig. 4 | Local positron spectrum. Data from AMS-02[108] and PAMELA (Payload for Antimatter Matter Exploration and Light-nuclei Astrophysics[109]), together with predictions from refs. [84,85], and the flux inferred in ref. [9]. Error bars represent 1σ statistical errors in the data points.

cosmic rays, and even put crucial constraints on the origin of the locally measured cosmic-ray fluxes. In this sense, it is important to understand how common pulsar haloes are[28,71].

Local effects. Electrons and positrons that escape from these sources can substantially contribute to the local all-electron ($e^{\pm}$) spectrum[72]. This provides information about the propagation of these $e^{\pm}$, while the e^{+} fraction (e^{+} flux divided by $e^{\pm}$ flux) provides the ratio between the flux of secondary positrons, produced in the collisions of cosmic rays with the ISM, and that of the dominant primary electrons. There is, however, an anomaly known as the 'positron excess' in the e^{+} fraction, produced by an excess of positrons above the cosmic-ray-induced background[73–75] above energies of a few gigaelectronvolts that has led to intense speculation on their origin. This excess has been postulated to arise from PWNe[76,77], microquasar jets[78] or dark-matter annihilation[79]. According to the most commonly accepted propagation theories within the ISM, the highest-energy positrons measured by satellites (~1 TeV) must originate from a region within a few kiloparsecs from the Earth ($r_{\rm d}(E) = \sqrt{2D(E)t_{\rm cool}}(E)$, where $D(1\,\mathrm{TeV}) \approx 10^{29}$–$10^{30}\,\mathrm{cm^{-2}\,s^{-1}}$, depending on the assumed energy dependence of the diffusion coefficient, and $t_{\rm cool}(1\,\mathrm{TeV}) \approx 300\,\mathrm{kyr}$, also depending on the assumed energy losses), limiting the number of possible sources behind this phenomenon[80].

In Figs. 3 and 4, we can see different estimations from the literature for the local all-electron and positron spectra; some other recent works on local electron/positron spectrum estimations can also be found in the literature[81–85]. The HAWC results on Geminga and PSR B0656+14[9] argued against a substantial contribution to the electron and positron spectra at the Earth by these two pulsars, assuming a uniform (one-zone) diffusion coefficient from them to the Earth. There has since been extensive literature arguing otherwise[85–88], by invoking a two-zone diffusion model to describe the propagation of these escaping electrons. In this scenario, the totality of the high-energy electrons and positrons measured at the Earth can be explained using nearby pulsars.

The recent measurement of the cosmic-ray all-electron spectrum up to ~20 TeV (ref. [89]), in addition to those by the Dark Matter Particle Explorer[90] and the Calorimetric Electron Telescope[91], indicates that these electrons and positrons must be generated near the Earth because of their cooling due to their interaction with interstellar magnetic and photon fields. Assuming fast diffusion, the origin of these high-energy electrons may be the aforementioned pulsars, or sources such as SNRs[92,93]. The key to discerning between these two source types is the positron flux, which seems to point to a decrease at the highest energies, disfavouring pulsars as the origin of the highest-energy electrons[94]. If, on the other hand, we consider a slower diffusion, even an undiscovered pulsar in the Local Bubble, the explanation of the local high-energy cosmic-ray all-electron spectrum might still be dominated by pulsars[95]. Another observable directly related to the local contribution of a particular source type is the dipole anisotropy, which should in principle pinpoint the origin of the primary accelerator. The current measurements are however still compatible with the different scenarios proposed[95,96].

It remains an open question whether known pulsars[97], SNRs[92], unknown pulsars[95] or dark matter[79] are still a viable explanation for the local $e^{\pm}$ flux.

Global effects. The level of magnetic field turbulence with respect to the average in the Milky Way is expected to increase in regions dominated by an active cosmic-ray accelerator[98], but it is difficult to find an efficient mechanism that could explain such an increase in the turbulence in the case of haloes around pulsars, as discussed in Implications in PWN theory. Assuming that the existence of pulsar haloes implies a slow diffusion coefficient, there are two scenarios in which the existence of pulsar haloes can affect the global propagation of cosmic rays in our Galaxy. First, we assume that this slow diffusion is only a signature of regions surrounding sources of this type. In this first scenario, if these haloes cover a large fraction of the Galaxy, they could substantially slow down Galactic cosmic-ray propagation. It is however unlikely that they can impact the

overall residence time of hadronic cosmic rays in the Galaxy, which is dominated by propagation in the halo[68,87]. The second scenario is the case where the diffusion coefficient derived from the observation of pulsar haloes is a more accurate representation of the average in the Galaxy. This may have profound implications, such as a much larger accumulated grammage by cosmic-ray nuclei (see, e.g., ref. [99] for a discussion of these effects around SNRs), which is in any case mostly determined by propagation in the disk, difficult to reconcile with the results obtained with cosmic-ray propagation codes such as GALPROP[100], DRAGON2[101], PICARD[102] or USINE[103]. This constraint must be carefully taken into account by 'Swiss-cheese'-like models of diffusion in the Galactic disk[88].

Conclusions and prospects

The 'pulsar–pulsar wind–pulsar wind nebula' concept is a successful paradigm explaining the link between two major galactic source populations: pulsars (compact relativistic objects) and PWNe (diffuse non-thermal structures filled by magnetic fields and relativistic electrons). The link is realized through the ultrarelativistic (most likely, cold) electron–positron wind with bulk motion Lorentz factor $\gamma \sim 10^5$–10^6. The typical magnetic field of almost all PWNe is rather modest—about 10 μG or even less (the Crab nebula is an atypical PWN; its average field of 200–300 μG is a rare exception—note also that magnetic fields higher than 10 μG have been inferred from modelling efforts; see, e.g., ref. [104]), but the general trend of low magnetic field holds. The favourable combination of the low magnetic field and injection of ultrarelativistic electrons at a rate comparable to the pulsar's spin-down luminosity allows electrons to travel tens of parsecs from their acceleration sites and form large-scale gamma-ray structures, which can be detected by the current ground-based instruments. In halo-type emission, we expect spherically symmetric morphology of gamma rays with radial distribution of electrons close to $1/r$ taking into account the continuous injection of electrons with a constant rate over $\geq 10^4$ yr. However, at the highest energies, the radiative losses become an essential factor, and we should see an energy cutoff toward the outskirts of the halo. The model-independent information about the spatial and spectral distribution of electrons provides a unique tool for the extraction of the diffusion coefficient characterizing the propagation of cosmic rays in the Galactic disk. The multi-hundred-teraelectronvolt electrons in the interstellar magnetic fields produce X-ray synchrotron extended sources. The detection of these objects with angular extensions of $\geq 1°$ is challenging but feasible, for bright gamma-ray haloes, by eROSITA, or planned experiments such as AMEGO (All-sky Medium Energy Gamma-ray Observatory) and AdEPT (The Advanced Energetic Pair Telescope)[105]. Thus, the combined X-ray and multi-teraelectronvolt observations could provide exact independent measurements of the interstellar magnetic field throughout the Galactic disk on ≤ 100 pc scales. Several authors[29,45,71] have computed prospects for the number of haloes that could be detected by current and future facilities, using different assumptions. This number ranges from a few, as currently detected, up to hundreds of haloes, under the most optimistic assumptions. It is expected that the next-generation detectors, in particular CTA and SWGO, together with the partly completed LHAASO, will markedly increase the number of identified pulsar haloes. Likewise, the continuous increment of the already vast Fermi-LAT dataset will increase the sensitivity to low-surface-brightness sources, not only unveiling more Geminga-like objects but also characterizing the spectrum in the sub-100-GeV energy range[106].

It would not be an exaggeration to argue that the very task of exploration of these standard candles, containing direct information about the energy budget of pulsars in the relativistic electrons, as well as about the cosmic-ray diffusion coefficient and the magnetic field strength in the ISM, would alone justify these ambitious ground-based projects.

Received: 18 June 2021; Accepted: 30 November 2021;
Published online: 14 February 2022

References

1. Weekes, T. C. et al. Observation of TeV gamma rays from the Crab nebula using the atmospheric Cerenkov imaging technique. *Astrophys. J.* **342**, 379–395 (1989).
2. Hester, J. J. The Crab nebula: an astrophysical chimera. *Annu. Rev. Astron. Astrophys.* **46**, 127–155 (2008).
3. Bühler, R. & Blandford, R. The surprising Crab pulsar and its nebula: a review. *Rep. Prog. Phys.* **77**, 066901 (2014).
4. Gaensler, B. M. & Slane, P. O. The evolution and structure of pulsar wind nebulae. *Annu. Rev. Astron. Astrophys.* **44**, 17–47 (2006).
5. Porth, O., Komissarov, S. S. & Keppens, R. Solution to the sigma problem of pulsar wind nebulae. *Mon. Not. R. Astron. Soc.* **431**, L48–L52 (2013).
6. Reynolds, S. P. Magnetohydrodynamic models for the structure of pulsar-wind nebulae. Preprint at https://arxiv.org/abs/astro-ph/0308483 (2003).
7. Del Zanna, L. & Olmi, B. in *Modelling Pulsar Wind Nebulae* (ed. Torres, D.) 215 (Astrophysics and Space Science Library Vol. 446, Springer, 2017).
8. Porth, O., Vorster, M. J., Lyutikov, M. & Engelbrecht, N. E. Diffusion in pulsar wind nebulae: an investigation using magnetohydrodynamic and particle transport models. *Mon. Not. R. Astron. Soc.* **460**, 4135–4149 (2016).
9. Abeysekara, A. U. et al. Extended gamma-ray sources around pulsars constrain the origin of the positron flux at Earth. *Science* **358**, 911–914 (2017).
10. Berezinskii, V. S., Bulanov, S. V., Dogiel, V. A. & Ptuskin, V. S. *Astrophysics of Cosmic Rays* (North Holland, 1990).
11. Trotta, R. et al. Constraints on cosmic-ray propagation models from a global Bayesian analysis. *Astrophys. J.* **729**, 106 (2011).
12. Aharonian, F. et al. A new population of very high energy gamma-ray sources in the Milky Way. *Science* **307**, 1938–1942 (2005).
13. Aharonian, F. et al. The H.E.S.S. survey of the Inner Galaxy in very high energy gamma rays. *Astrophys. J.* **636**, 777–797 (2006).
14. H.E.S.S. Collaboration et al. The H.E.S.S. Galactic plane survey. *Astron. Astrophys.* **612**, A1 (2018).
15. H.E.S.S. Collaboration et al. The population of TeV pulsar wind nebulae in the H.E.S.S. Galactic Plane Survey. *Astron. Astrophys.* **612**, A2 (2018).
16. Aharonian, F. A., Atoyan, A. M. & Kifune, T. Inverse Compton gamma radiation of faint synchrotron X-ray nebulae around pulsars. *Mon. Not. R. Astron. Soc.* **291**, 162–176 (1997).
17. Aleksić, J. et al. Discovery of TeV γ-ray emission from the pulsar wind nebula 3C 58 by MAGIC. *Astron. Astrophys.* **567**, L8 (2014).
18. Coerver, A. et al. Multiwavelength investigation of pulsar wind nebula DA 495 with HAWC, VERITAS, and NuSTAR. *Astrophys. J.* **878**, 126 (2019).
19. H.E.S.S. Collaboration, et al.An extreme particle accelerator in the Galactic plane: HESS J1826-130. *Astron. Astrophys.* **644**, A112 (2020).
20. H.E.S.S. Collaboration, et al.H.E.S.S. and Suzaku observations of the Vela X pulsar wind nebula. *Astron. Astrophys.* **627**, A100 (2019).
21. H.E.S.S. Collaboration, et al.Identification of HESS J1303-631 as a pulsar wind nebula through γ-ray, X-ray, and radio observations. *Astron. Astrophys.* **548**, A46 (2012).
22. Principe, G. et al. Energy dependent morphology of the pulsar wind nebula HESS J1825-137 with Fermi-LAT. *Astron. Astrophys.* **640**, A76 (2020).
23. Abdo, A. A. et al. TeV gamma-ray sources from a survey of the Galactic plane with Milagro. *Astrophys. J. Lett.* **664**, L91–L94 (2007).
24. Albert, A. et al. 3HWC: The Third HAWC Catalog of Very-high-energy Gamma-Ray Sources. *Astrophys. J.* **905**, 76 (2020).
25. Cao, Z. et al. Ultrahigh-energy photons up to 1.4 petaelectronvolts from 12 γ-ray Galactic sources. *Nature* **594**, 33–36 (2021).
26. Abdollahi, S. et al. Fermi Large Area Telescope Fourth Source Catalog. *Astrophys. J. Suppl. Ser.* **247**, 33 (2020).
27. Recchia, S. et al. Do the Geminga, Monogem and PSR J0622+3749 γ-ray halos imply slow diffusion around pulsars? *Phys. Rev. D* **104**, 123017 (2021).
28. Giacinti, G. et al. Halo fraction in TeV-bright pulsar wind nebulae. *Astron. Astrophys.* **636**, A113 (2020).
29. Linden, T. et al. Using HAWC to discover invisible pulsars. *Phys. Rev. D* **96**, 103016 (2017).
30. H.E.S.S. Collaboration, et al.Particle transport within the pulsar wind nebula HESS J1825-137. *Astron. Astrophys.* **621**, A116 (2019).
31. Khangulyan, D., Koldoba, A. V., Ustyugova, G. V., Bogovalov, S. V. & Aharonian, F. On the anomalously large extension of the pulsar wind nebula HESS J1825-137. *Astrophys. J.* **860**, 59 (2018).
32. Rishbeth, H. Radio emission from the Vela–Puppis region. *Aust. J. Phys.* **11**, 550–563 (1958).
33. Aharonian, F. et al. First detection of a VHE gamma-ray spectral maximum from a cosmic source: HESS discovery of the Vela X nebula. *Astron. Astrophys.* **448**, L43–L47 (2006).

34. Tibaldo, L. et al. Disentangling multiple high-energy emission components in the Vela X pulsar wind nebula with the Fermi Large Area Telescope. *Astron. Astrophys.* **617**, A78 (2018).
35. Grondin, M. H. et al. The Vela-X pulsar wind nebula revisited with four years of Fermi Large Area Telescope observations. *Astrophys. J.* **774**, 110 (2013).
36. Mitchell, A. (for the H.E.S.S. Collaboration) *Search for Extended Gamma-ray Emission Around the Geminga Pulsar with H.E.S.S* (2019).
37. Flinders, A. VERITAS observations of the Geminga supernova remnant. Preprint at https://arxiv.org/abs/1509.04224 (2015).
38. Ahnen, M. L. et al. Search for VHE gamma-ray emission from Geminga pulsar and nebula with the MAGIC telescopes. *Astron. Astrophys.* **591**, A138 (2016).
39. Riviere, C., Fleischhack, H. & Sandoval, A. HAWC detection of TeV emission near PSR B0540+23. *The Astronomer's Telegram* **10941** (2017).
40. Brisbois, C., Riviere, C., Fleischhack, H. & Smith, A. HAWC detection of TeV source HAWC J0635+070. *The Astronomer's Telegram* **12013** (2018).
41. Smith, A. A systematic search for TeV halos associated with known pulsars. *PoS* **ICRC2019**, 797 (2019).
42. Abeysekara, A. U. et al. Multiple Galactic sources with emission above 56 TeV detected by HAWC. *Phys. Rev. Lett.* **124**, 021102 (2020).
43. LHAASO Collaboration. Extended very-high-energy gamma-ray emission surrounding PSR J0622+3749 observed by LHAASO-KM2A. *Phys. Rev. Lett.* **126**, 241103 (2021).
44. Hooper, D. & Linden, T. Measuring the local diffusion coefficient with H.E.S.S. observations of very high-energy electrons. *Phys. Rev. D* **98**, 083009 (2018).
45. Di Mauro, M., Manconi, S. & Donato, F. Evidences of low-diffusion bubbles around Galactic pulsars. *Phys. Rev. D* **101**, 103035 (2020).
46. Chen, S. (for the LHAASO Collaboration) *LHAASO Performance and First Results on Extended Emission from Known Halos* (2020).
47. Guo, Y. Observations of extended very-high-energy halos around Geminga and Monogem with the LHAAS0-KM2A. *PoS* **ICRC2021**, 964 (2021).
48. Caraveo, P. A. et al. Geminga's tails: a pulsar bow shock probing the interstellar medium. *Science* **301**, 1345–1348 (2003).
49. Posselt, B. et al. Geminga's puzzling pulsar wind nebula. *Astrophys. J.* **835**, 66 (2017).
50. Di Mauro, M., Manconi, S. & Donato, F. Detection of a γ-ray halo around Geminga with the Fermi-LAT data and implications for the positron flux. *Phys. Rev. D* **100**, 123015 (2019).
51. Xi, S.-Q., Liu, R.-Y., Huang, Z.-Q., Fang, K. & Wang, X.-Y. GeV observations of the extended pulsar wind nebulae constrain the pulsar interpretations of the cosmic-ray positron excess. *Astrophys. J.* **878**, 104 (2019).
52. Johnson, S. P. & Wang, Q. D. The pulsar B2224+65 and its jets: a two epoch X-ray analysis. *Mon. Not. R. Astron. Soc.* **408**, 1216–1224 (2010).
53. Hui, C. Y. et al. XMM-Newton observation of PSR B2224+65 and its jet. *Astrophys. J.* **747**, 74 (2012).
54. Pavan, L. et al. The long helical jet of the Lighthouse nebula, IGR J11014-6103. *Astron. Astrophys.* **562**, A122 (2014).
55. Liu, R.-Y., Ge, C., Sun, X.-N. & Wang, X.-Y. Constraining the magnetic field in the TeV halo of Geminga with X-ray observations. *Astrophys. J.* **875**, 149 (2019).
56. Goldreich, P. & Julian, W. H. Pulsar electrodynamics. *Astrophys. J.* **157**, 869 (1969).
57. Sironi, L., Keshet, U. & Lemoine, M. Relativistic shocks: particle acceleration and magnetization. *Space Sci. Rev.* **191**, 519–544 (2015).
58. Sironi, L. & Spitkovsky, A. Acceleration of particles at the termination shock of a relativistic striped wind. *Astrophys. J.* **741**, 39 (2011).
59. Hoshino, M., Arons, J., Gallant, Y. A. & Langdon, A. B. Relativistic magnetosonic shock waves in synchrotron sources: shock structure and nonthermal acceleration of positrons. *Astrophys. J.* **390**, 454 (1992).
60. Amato, E. & Arons, J. Heating and nonthermal particle acceleration in relativistic, transverse magnetosonic shock waves in proton–electron–positron plasmas. *Astrophys. J.* **653**, 325–338 (2006).
61. Amato, E. The theory of pulsar wind nebulae: recent progress. Preprint at https://arxiv.org/abs/2001.04442 (2020).
62. Olmi, B., Del Zanna, L., Amato, E., Bucciantini, N. & Mignone, A. Multi-D magnetohydrodynamic modelling of pulsar wind nebulae: recent progress and open questions. *J. Plasma Phys.* **82**, 635820601 (2016).
63. Olmi, B. & Bucciantini, N. Full-3D relativistic MHD simulations of bow shock pulsar wind nebulae: dynamics. *Mon. Not. R. Astron. Soc.* **484**, 5755–5770 (2019).
64. Olmi, B. & Bucciantini, N. On the origin of jet-like features in bow shock pulsar wind nebulae. *Mon. Not. R. Astron. Soc.* **490**, 3608–3615 (2019).
65. Kulsrud, R. & Pearce, W. P. The effect of wave–particle interactions on the propagation of cosmic rays. *Astrophys. J.* **156**, 445–469 (1969).
66. Evoli, C., Linden, T. & Morlino, G. Self-generated cosmic-ray confinement in TeV halos: implications for TeV γ-ray emission and the positron excess. *Phys. Rev. D* **98**, 063017 (2018).
67. Bell, A. R. Turbulent amplification of magnetic field and diffusive shock acceleration of cosmic rays. *Mon. Not. R. Astron. Soc.* **353**, 550–558 (2004).
68. López-Coto, R. & Giacinti, G. Constraining the properties of the magnetic turbulence in the Geminga region using HAWC γ-ray data. *Mon. Not. R. Astron. Soc.* **479**, 4526–4534 (2018).
69. Strong, A. W., Moskalenko, I. V. & Ptuskin, V. S. Cosmic-ray propagation and interactions in the galaxy. *Annu. Rev. Nucl. Part. Sci.* **57**, 285–327 (2007).
70. Grenier, I. A., Black, J. H. & Strong, A. W. The nine lives of cosmic rays in galaxies. *Annu. Rev. Astron. Astrophys.* **53**, 199–246 (2015).
71. Sudoh, T., Linden, T. & Beacom, J. F. TeV halos are everywhere: prospects for new discoveries. *Phys. Rev. D* **100**, 043016 (2019).
72. Atoyan, A. M., Aharonian, F. A. & Völk, H. J. Electrons and positrons in the galactic cosmic rays. *Phys. Rev. D* **52**, 3265–3275 (1995).
73. Adriani, O. et al. An anomalous positron abundance in cosmic rays with energies 1.5–100 GeV. *Nature* **458**, 607–609 (2009).
74. Ackermann, M. et al. Measurement of separate cosmic-ray electron and positron spectra with the Fermi Large Area Telescope. *Phys. Rev. Lett.* **108**, 011103 (2012).
75. Aguilar, M. et al. First result from the Alpha Magnetic Spectrometer on the International Space Station: precision measurement of the positron fraction in primary cosmic rays of 0.5–350 GeV. *Phys. Rev. Lett.* **110**, 141102 (2013).
76. Aharonian, F. A., Atoyan, A. M. & Voelk, H. J. High energy electrons and positrons in cosmic rays as an indicator of the existence of a nearby cosmic tevatron. *Astron. Astrophys.* **294**, L41–L44 (1995).
77. Yüksel, H., Kistler, M. D. & Stanev, T. TeV gamma rays from Geminga and the origin of the GeV positron excess. *Phys. Rev. Lett.* **103**, 051101 (2009).
78. Gupta, N. & Torres, D. F. pγ interactions in Galactic jets as a plausible origin of the positron excess. *Mon. Not. R. Astron. Soc.* **441**, 3122–3126 (2014).
79. Bergström, L., Bringmann, T. & Edsjö, J. New positron spectral features from supersymmetric dark matter: a way to explain the PAMELA data? *Phys. Rev. D* **78**, 103520 (2008).
80. Evoli, C., Amato, E., Blasi, P. & Aloisio, R. Galactic factories of cosmic-ray electrons and positrons. *Phys. Rev. D* **103**, 083010 (2021).
81. Lipari, P. Interpretation of the cosmic ray positron and antiproton fluxes. *Phys. Rev. D* **95**, 063009 (2017).
82. Lipari, P. Spectral shapes of the fluxes of electrons and positrons and the average residence time of cosmic rays in the Galaxy. *Phys. Rev. D* **99**, 043005 (2019).
83. Evoli, C., Blasi, P., Amato, E. & Aloisio, R. Signature of energy losses on the cosmic ray electron spectrum. *Phys. Rev. Lett.* **125**, 051101 (2020).
84. Evoli, C., Amato, E., Blasi, P. & Aloisio, R. Galactic factories of cosmic-ray electrons and positrons. *Phys. Rev. D* **103**, 083010 (2021).
85. Manconi, S., Di Mauro, M. & Donato, F. Contribution of pulsars to cosmic-ray positrons in light of recent observation of inverse-Compton halos. *Phys. Rev. D* **102**, 023015 (2020).
86. Jóhannesson, G., Porter, T. A. & Moskalenko, I. V. Cosmic-ray propagation in light of the recent observation of Geminga. *Astrophys. J.* **879**, 91 (2019).
87. Hooper, D., Cholis, I., Linden, T. & Fang, K. HAWC observations strongly favor pulsar interpretations of the cosmic-ray positron excess. *Phys. Rev. D* **96**, 103013 (2017).
88. Profumo, S., Reynoso-Cordova, J., Kaaz, N. & Silverman, M. Lessons from HAWC pulsar wind nebulae observations: the diffusion constant is not a constant; pulsars remain the likeliest sources of the anomalous positron fraction; cosmic rays are trapped for long periods of time in pockets of inefficient diffusion. *Phys. Rev. D* **97**, 123008 (2018).
89. Kerszberg, D. (for the H. E. S. S. Collaboration) *The Cosmic-ray Electron Spectrum Measured with H.E.S.S* (2017).
90. DAMPE Collaboration et al. Direct detection of a break in the teraelectronvolt cosmic-ray spectrum of electrons and positrons. *Nature* **552**, 63–66 (2017).
91. Adriani, O. et al. Energy spectrum of cosmic-ray electron and positron from 10 GeV to 3 TeV observed with the Calorimetric Electron Telescope on the International Space Station. *Phys. Rev. Lett.* **119**, 181101 (2017).
92. Recchia, S., Gabici, S., Aharonian, F. A. & Vink, J. Local fading accelerator and the origin of TeV cosmic ray electrons. *Phys. Rev. D* **99**, 103022 (2019).
93. Fornieri, O., Gaggero, D. & Grasso, D. Features in cosmic-ray lepton data unveil the properties of nearby cosmic accelerators. *J. Cosmol. Astropart. Phys.* **2020**, 009 (2020).
94. Aguilar, M. et al. Towards understanding the origin of cosmic-ray electrons. *Phys. Rev. Lett.* **122**, 101101 (2019).
95. López-Coto, R., Parsons, R. D., Hinton, J. A. & Giacinti, G. Undiscovered pulsar in the Local Bubble as an explanation of the local high energy cosmic ray all-electron spectrum. *Phys. Rev. Lett.* **121**, 251106 (2018).
96. Manconi, S., Di Mauro, M. & Donato, F. Dipole anisotropy in cosmic electrons and positrons: inspection on local sources. *J. Cosmol. Astropart. Phys.* **1**, 006 (2017).

97. Manconi, S., Di Mauro, M. & Donato, F. Multi-messenger constraints to the local emission of cosmic-ray electrons. Preprint at https://arxiv.org/abs/1803.01009 (2018).
98. Ackermann, M. et al. A cocoon of freshly accelerated cosmic rays detected by Fermi in the Cygnus superbubble. *Science* **334**, 1103 (2011).
99. D'Angelo, M., Blasi, P. & Amato, E. Grammage of cosmic rays around Galactic supernova remnants. *Phys. Rev. D* **94**, 083003 (2016).
100. Strong, A. W. & Moskalenko, I. V. Propagation of cosmic-ray nucleons in the galaxy. *Astrophys. J.* **509**, 212–228 (1998).
101. Evoli, C. et al. Cosmic-ray propagation with DRAGON2: I. Numerical solver and astrophysical ingredients. *J. Cosmol. Astropart. Phys.* **2017**, 015 (2017).
102. Kissmann, R. PICARD: a novel code for the Galactic cosmic ray propagation problem. *Astropart. Phys.* **55**, 37–50 (2014).
103. Maurin, D., Donato, F., Taillet, R. & Salati, P. Cosmic rays below $Z=30$ in a diffusion model: new constraints on propagation parameters. *Astrophys. J.* **555**, 585–596 (2001).
104. Bucciantini, N., Arons, J. & Amato, E. Modelling spectral evolution of pulsar wind nebulae inside supernova remnants. *Mon. Not. R. Astron. Soc.* **410**, 381–398 (2011).
105. Di Mauro, M., Manconi, S. & Donato, F. Prospects for the detection of synchrotron halos around middle-age pulsars. *Bull. Am. Astron. Soc.* **51**, 183 (2019).
106. Bonnarel, F. et al. The ALADIN interactive sky atlas. A reference tool for identification of astronomical sources. *Astron. Astrophys. Suppl.* **143**, 33–40 (2000).
107. Abdollahi, S. et al. Cosmic-ray electron–positron spectrum from 7 GeV to 2 TeV with the Fermi Large Area Telescope. *Phys. Rev. D* **95**, 082007 (2017).
108. Aguilar, M. et al. Towards understanding the origin of cosmic-ray positrons. *Phys. Rev. Lett.* **122**, 041102 (2019).
109. Adriani, O. et al. Cosmic-ray positron energy spectrum measured by PAMELA. *Phys. Rev. Lett.* **111**, 081102 (2013).

Acknowledgements

This article is the result of fruitful discussions during the First Workshop on Gamma-ray Halos Around Pulsars (https://agenda.infn.it/e/GammaHalos). We first and foremost thank the Scientific Organizing Committee of the Workshop (A. Mitchell, S. Profumo, D. Torres, H. Zhou, R. Zanin), the Local Organizing Committee (M. I. Bernardos, A. de Angelis, A. Spolon) and all the participants (S. Abdollahi, A. Abdulrahman, F. Acero, F. Aharonian, A. Albert, E. Amato, M. Araya, T. Armstrong, V. Baghmanyan, C. Baheeja, A. Baktash, Y. Bao, M. Barnard, U. Barres de Almeida, I. Batkovic, M. Bernardos Martin, P. Blasi, P. Blay, M. Breuhaus, C. Brisbois, D. Burgess, S. Çabuk, F. Calore, T. Capistran Rojas, P. Caraveo, M. Cardillo, A. Carramiñana, M. Carreon Gonzalez, S. Casanova, F. Cassol, S. Chagren, P. Chambery, T. Chand, S. Chen, J.-G. Cheng, S. M. Colak, H. Costantini, R. Crocker, A. De Angelis, E. de la Fuente Acosta, E. de Oña Wilhelmi, A. De Sarkar, J. Devin, M. Di Mauro, B. Dingus, F. Donato, J. Eagle, C. Eckner, K. Egberts, G. Emery, A. Eungwanichayapant, C. Evoli, Y. Eweis, K. L. Fan, K. Fang, L. Fariña, Y. Feng, M. Fiori, H. Fleischhack, O. Fornieri, Y. Gallant, G. Giacinti, M. Gonzalez, E. Gotthelf, J. Goulart Coelho, D. Green, I. Grenier, P. Grespan, M.-H. Grondin, Y. Guo, N. Gupta, A. Hahn, H. Hamed, I. Herzog, J. Hinton, B. Hnatyk, W. Hofmann, B. Hona, D. Huang, Z. Huang, A. Jardin-Blicq, H. Jiachun, H. Jiankun, G. Johannesson, V. Joshi, F. Kamal Youssef, G. Kanbach, D. Khangulyan, B. Khelifi, S. Kisaka, T. Kleiner, J. Knödlseder, D. Kostunin, A. Kundu, M. Kuss, P. C. W. Lai, S. Lalkovski, F. Lavorenti, M. Lemoine-Goumard, F. Leone, M. Linares, T. Linden, R. Liu, S. Lloyd, R. López-Coto, I. Lypova, K. Malone, S. Manconi, V. Marandon, A. Marcowith, J. Martin, P. Martin, F. Massaro, R. Mirzoyan, A. Mitchell, K. Mori, G. Morlino, R. Mukherjee, K. Nakashima, L. Nava, A. Nayerhoda, M. Newbold, M. Nynka, B. Olmi, E. Orlando, Z. Ou, M. Pilia, F. Pintore, I. Plotnikov, T. Porter, R. R. Prado, E. Prandini, G. Principe, S. Profumo, H. Rahman K. K., B. Reville, C. Righi, G. Rodríguez Fernández, L. Romanato, B. Rudak, S. Safi-Harb, T. Saito, A. Sandoval, A. Scherer, P. Sharma, S. Silvestri, A. Sinha, H. Spackman, A. Spolon, G. Stratta, A. Strong, M. Strzys, T. Sudoh, X. Sun, P. H. T. Tam, S. Tanaka, F. Tavecchio, R. Terrier, L. Tibaldo, G. Tingting, D. Torres, R. Torres Escobedo, M. Tsirou, N. Tsuji, A. Tutone, A. J. van Marle, J. van Scherpenberg, G. Verna, J. Vink, E. Vurgun, S. M. Wagner, J. Wang, X. Wang, J. Xia, G. Zaharijas, S. Zane, R. Zanin, D. Zargaryan, D. Zaric, J. Zhang, Y. Zhang, Y. Zhang, H. Zhou).

R.L.-C. acknowledges the financial support of the European Union Horizon 2020 research and innovation programme under the Marie Skłodowska-Curie grant agreement 754496-FELLINI. R.L.-C. also acknowledges financial support from the State Agency for Research of the Spanish MCIU through the Centre of Excellence Severo Ochoa award to the Instituto de Astrofísica de Andalucía (SEV-2017-0709). E.A. acknowledges support from ASI-INAF under grant 2017-14-H.0) and from INAF under grants PRIN SKA-CTA, INAF Mainstream 2018 and PRIN-INAF 2019.

Author contributions

R.L.-C. and E.d.O.W. coordinated the manuscript writing. All authors meet the journal's authorship criteria and have reviewed, discussed and commented on the content of the Review.

Competing interests

The authors declare no competing interests.

Additional information

Correspondence should be addressed to Rubén López-Coto or Emma de Oña Wilhelmi.

Peer review information *Nature Astronomy* thanks Mattia Di Mauro, Patrick Slane and the other, anonymous, reviewer(s) for their contribution to the peer review of this work.